Optical Solitons Carrying Orbital Angular Momentum

W. J. Firth and D. V. Skryabin*

Department of Physics and Applied Physics, John Anderson Building, University of Strathclyde, 107 Rottenrow, Glasgow, G4 0NG, United Kingdom

(Received 10 April 1997; revised manuscript received 1 July 1997)

We predict a new kind of ring-profile solitary wave in nonlinear optical media, with finite orbital angular momentum. During propagation these fragment into fundamental solitons. Like free Newtonian particles, these fly off tangential to the ring, vividly demonstrating conservation of orbital angular momentum in soliton motion. [S0031-9007(97)04148-3]

PACS numbers: 42.65.Tg, 03.40.Kf, 42.65.Ky

Solitons are important in many branches of science [1]. They are nonlinear waves which possess several mechanical and other attributes more commonly associated with particles. This analogy is usually developed in relation to their response to external "forces," i.e., in the context of linear momentum; see, e.g., [2]. Here we describe phenomena which are neatly interpreted as solitons carrying *orbital angular* momentum, arising from motion oblique to the centroid of the system.

These solitons are produced in the fragmentation of a new kind of "doughnut soliton." They have well-defined angular momentum which is transformed into orbital angular momentum of the daughter solitons. Below we demonstrate this phenomenon in two rather different nonlinear optical systems. The close correspondence of the dynamics in the two cases lead us to believe that this scenario should be quite general in solitonic systems with enough dimensions to exhibit angular momentum effects.

Our first model, $\chi^{(3)}$, describes a beam propagating in a saturable self-focusing medium. In the paraxial approximation the evolution in z of the field envelope $E_1(x, y, z)$ obeys the following dimensionless equation [3]

$$i\partial_z E_1 + \frac{1}{2}\vec{\nabla}_\perp^2 E_1 + E_1|E_1|^2/(1 + \alpha|E_1|^2) = 0. \quad (1)$$

Here $\vec{\nabla}_\perp = \vec{i}\partial_x + \vec{j}\partial_y$. For a pure Kerr medium ($\alpha = 0$) this equation is the well-known nonlinear Schrödinger equation (NLS). With the y-dimension suppressed (1D case) the NLS is integrable, with exact solutions—solitons—of sech profile. In 2D it has solitonlike solutions which are unstable, collapsing to a singularity [3]. Saturation, described by a finite positive α, prevents this collapse [3]. Thus, though it is not integrable, Eq. (1) possesses stable solitary wave solutions, localized in 2D, which we will term "solitons."

Our second model, $\chi^{(2)}$, is physically different, corresponding to the coupled propagation of an optical field and its second harmonic in a quadratically nonlinear medium. Their field envelopes E_1 and E_2 can be described by the following system of rescaled equations [4]:

$$\begin{aligned} i\partial_z E_1 + \frac{1}{2}\vec{\nabla}_\perp^2 E_1 + E_1^* E_2 &= 0, \\ i\partial_z E_2 + \frac{1}{4}\vec{\nabla}_\perp^2 E_2 + \frac{1}{2}E_1^2 &= \beta E_2. \end{aligned} \quad (2)$$

A recent review [5] provides a good link to experimental parameters, and to complications such as field polarization and walk-off which we neglect here. The parameter β is the phase mismatch. If β is large enough, it can be considered to dominate the derivative terms, then solving for E_2 and substituting into the equation for E_1 gives the NLS. Again Eqs. (2) are not integrable, but stable solitary solutions persist even for small β, far from the NLS limit. We present results for $\beta = 0$ in the following: the phenomena we describe are not very sensitive to β. These solitons are now well known both experimentally and theoretically; see [4–6] and *op cit.*

All quantities in Eqs. (1) and (2) are dimensionless, and these scaled units are used throughout the text and in the figures. Note that both equations have a Galilean invariance, and so the 2D spatial soliton centered on $(x = 0, y = 0)$ generates a family of equivalent solitons which "move" with constant velocity in the (x, y) plane as the beam propagates. It is such moving solitons which are important in the following.

Both models are Hamiltonian, and possess phase, translational, and rotational symmetries. As a consequence, both conserve the energy integral Q, transverse momentum $\vec{P}$, and transverse angular momentum $\vec{L}$, defined as follows: $Q = \int dxdy(|E_1|^2 + 2|E_2|^2)$, $\vec{P} = \int dxdy\,\vec{p} = \int dxdy\frac{i}{2}[E_1(\vec{\nabla}_\perp \cdot E_1^*) + E_2(\vec{\nabla}_\perp \cdot E_2^*) - \text{c.c.}]$, $\vec{L} = \int dxdy\,\vec{r} \times \vec{p}$, where $\vec{p}$ is the transverse momentum density and $\vec{r}$ is the transverse radius vector. (For the $\chi^{(3)}$ model set E_2 to zero.)

The angular momentum carried by light beams has attracted much recent interest. It has been predicted, and proved experimentally, that Laguerre-Gaussian beams with azimuthal model index l carry orbital angular momentum $l\hbar$ per photon [7]. Frequency doubling such a

 0031-9007/97/79(13)/2450(4)$10.00

beam has been shown [8] to generate a second harmonic with doubled azimuthal mode index $2l$.

We now show that both our models admit nondiffracting solitary wave solutions with finite angular momentum. Such "doughnut solitons" are ringlike solutions of (1) or (2) with intensity independent of z. Equations (1) and (2) are reduced by the substitution $E_m(z, r, \theta) = A_m(r) \exp[im(\kappa z + l\theta)]$ $(m = 1, 2)$ to ordinary differential equations which we solve numerically using finite differences. Here $r = \sqrt{x^2 + y^2}$, θ is the polar angle, κ is a real and free parameter, as is l, which we restrict to integer values to ensure azimuthal periodicity. $A_{1,2}(r)$ are real functions which satisfy zero boundary conditions: $A_{1,2}(0) = A_{1,2}(+\infty) = 0$. For the $\chi^{(3)}$ model, consider $m = 1$ only (here and below).

For each l, $\chi^{(3)}$ doughnut solitons exist for all positive κ (which is required for soliton confinement), while for $\chi^{(2)}$ the existence condition is $\kappa > \max(0, -\beta/2)$. Doughnut solitons obey $\vec{P} = 0$ and $|\vec{L}| = |l|Q$ in both models. Typical spatial profiles are presented in Figs. 1(a) and 1(b).

To investigate doughnut soliton stability under propagation, we initialize (1) or (2) with a doughnut soliton (plus noise) and simulate the subsequent evolution on both Cartesian and polar grids, using split-step algorithms. Both approaches give the same results. As a further check, conservation of the energy, momentum, and angular momentum was monitored during the simulations. We find that these doughnuts usually break up into several solitons, which move off at constant "velocity" (angle to the axis of propagation) along paths tangent to the initial ring. The breakup is due to an azimuthal modulational instability. Before discussing the asymptotic motion of the "daughter" solitons, therefore, we outline our doughnut soliton stability analysis.

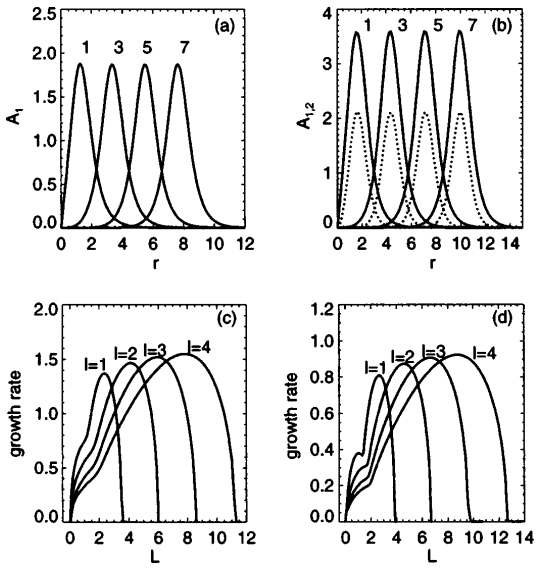

FIG. 1. (a) One-ring solitary wave solutions of Eq. (1): plots of the field amplitude $A_1(r)$ for $\kappa = 1$ and $l = 1, 3, 5, 7$. (b) Corresponding plots of $A_1(r)$ (full) and $A_2(r)$ (dotted) for Eqs. (2). (c) Perturbation growth rate $\mathrm{Re}\tilde{\lambda}$ vs L for different values of l, for the $\chi^{(3)}$ case; $\kappa = 1$, $\alpha = 0.1$. (d) Corresponding plots for the $\chi^{(2)}$ case; $\kappa = 1$, $\beta = 0$.

As regards radial perturbations, the criterion $\partial_\kappa Q > 0$ [9] for stability applies to the doughnut solitons, and is satisfied over most of the existence domain. However, $\partial_\kappa Q > 0$ does not imply stability with respect to azimuthal perturbations [10], which break the cylindrical symmetry. We therefore considered azimuthally perturbed doughnut solitons in the general form $E_m = [A_m(r) + \epsilon_m^+(r, z)e^{iL\theta} + \epsilon_m^-(r, z)e^{-iL\theta}]e^{im(\kappa z + l\theta)}$ $(m = 1, 2)$. Substitution into (1) or (2) and linearization results in partial differential equations for $\epsilon_{1,2}^{\pm}(r, z)$ which we solve numerically using a Crank-Nicholson scheme. We integrate along z until the perturbation growth rate becomes stationary and then average it over a further propagation distance. This procedure gives us an estimate for the real part of the maximally unstable eigenvalue $\tilde{\lambda}$. Alternatively, setting $\epsilon_{1,2}^{\pm} = [u_{1,2}^{\pm}(r) + iv_{1,2}^{\pm}(r)]e^{\lambda z}$ yields a boundary value problem whose spectrum we find by a finite difference method. The two methods give identical results.

Dependencies of the perturbation growth rate $\mathrm{Re}\tilde{\lambda}$ on L for various values of l with other parameters fixed are presented in Figs. 1(c) and 1(d). Physically, L must be an integer to ensure azimuthal periodicity, but it appears in the linearized equations as a real parameter, and extra insight can be gained by studying growth rates for arbitrary positive L. In every case there is a positive growth rate over a range of L values, with a well-defined global maximum for $L = L_{\max}$. We find that azimuthal instability $(L \neq 0)$ always dominates radial instability which corresponds to $L = 0$. On propagation, we expect the initially uniform field amplitude around the doughnut to develop N minima and N maxima, where N is the integer closest to $L_{\max}$. As a consequence, the doughnut should break up into N solitons. In the cases illustrated below $N = 2|l|$ for the $\chi^{(3)}$ model and $2|l| + 1$ for $\chi^{(2)}$.

We present results of direct numerical simulation of Eqs. (1) and (2) in Figs. 2 and 3, respectively, for the cases $l = 1, 2, 3$. Figures 2(a)–2(c) and 3(a)–3(c) show the real part of the perturbation eigenmode corresponding to $L = N$ computed from the stability analysis—the real part determines the field amplitude modulation pattern which develops around the initial ring. Figures 2(d)–2(f) and 3(d)–3(f) show the field intensity after propagating far enough for the modulational instability to develop. Each of the N peaks of the eigenmode evolves into an intensity peak (a protosoliton). (For the $\chi^{(2)}$ case the field amplitudes E_1, E_2 are localized in the same region of space due to their nonlinear coupling.)

Figures 2(g)–2(j) and 3(g)–3(j) show the real part of E_1, indicating that adjacent protosolitons are out of phase (this is less obvious in Fig. 3 because N is odd).

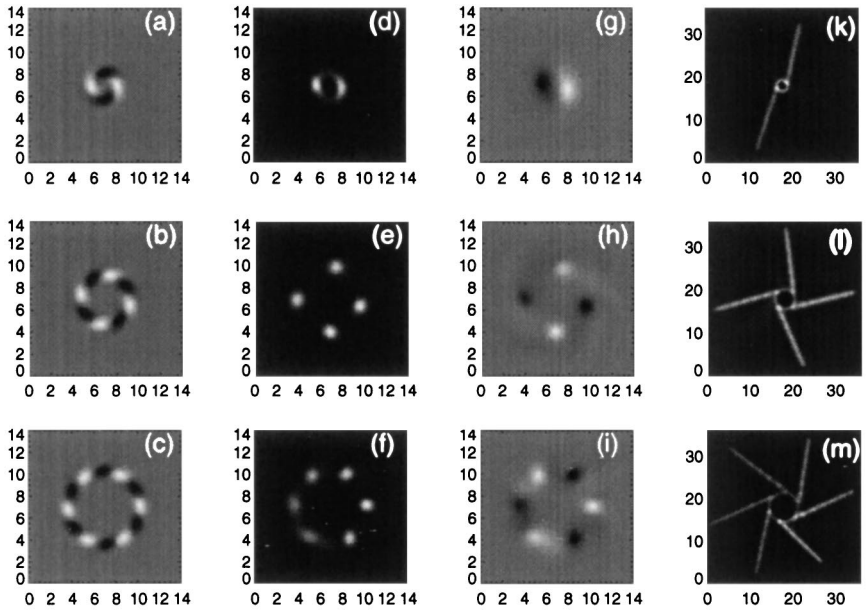

FIG. 2. Azimuthal modulational instability development and soliton trajectories, for $\chi^{(3)}$ case: $\alpha = 0.1$, $\kappa = 1$, with $l = 1, 2, 3$. (a)–(c) Real part of the perturbation field pattern with maximal growth rate. (d)–(f) Numerically computed field intensity $|E_1|^2$ at a point where protosolitons have developed. (g)–(i) Real part of E_1 at the same point, showing relative phases of protosolitons. (k)–(m) Superimposed images of the transverse intensity distribution at different z values, showing soliton trajectories tangential to the initial ring. Note the change of scale.

It has been noted that out-of-phase solitons repel each other, while in-phase attract; see, e.g., Ref. [11]. By symmetry, the resultant force on each protosoliton should thus be *radial* and outward. In Figs. 2(k)–2(m) and 3(k)–3(m) we superimpose a succession of images at different z, to show the daughter soliton trajectories. Far from being radial, these are *tangential* to the initial ring.

Our interpretation is that the intersoliton forces are actually negligible, and that the solitons are behaving like free Newtonian particles, flying off tangential to the doughnut soliton ring, and carrying away its angular momentum *via* the obliquity of their paths. The "mass" of the nth soliton is its energy Q_n, and its angular momentum is $\vec{r}_n \times \vec{p}_n$, where Q_n and $\vec{p}_n$ are now defined *locally* around the nth soliton's position $\vec{r}_n$. Using conservation of energy and angular momentum and the Galilean invariance of Eqs. (1) and (2) we calculate the transverse speed of the solitons to be $|\vec{v}| = |l|/R$, where

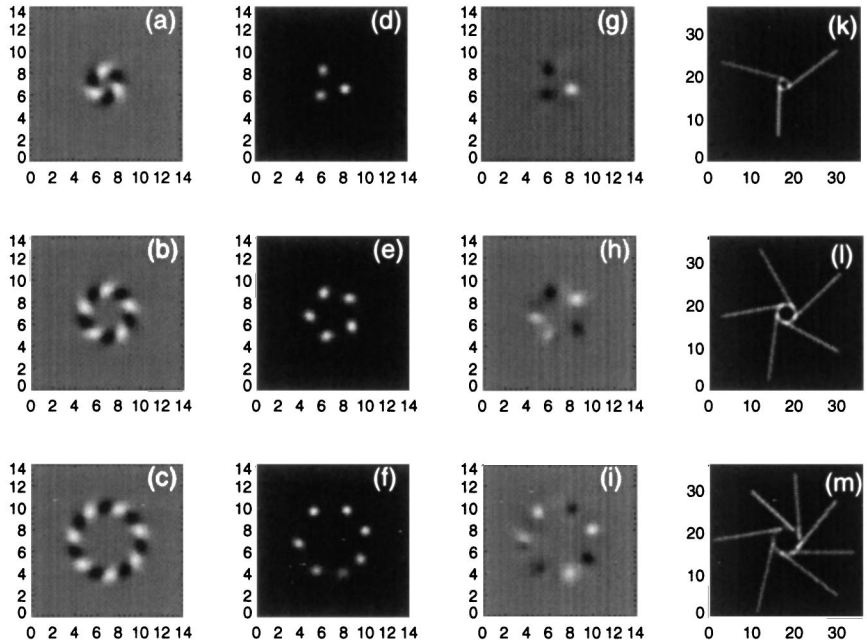

FIG. 3. Same as Fig. 2, but for field E_1 in the $\chi^{(2)}$ model: $\beta = 0$, $\kappa = 2$.

R is the radius of the initial doughnut (the same speed for each daughter soliton, independent of its energy).

This estimate is in good agreement with the numerical results shown in Figs. 2 and 3, with losses (due to nonsoliton "radiation") at most 10%. Thus, in contrast to recent work [11] in which interacting photorefractive solitons spiraled around each other, here we have nearly free solitons, with dynamics dominated by angular momentum conservation. Interactions forces may play a minor role in partitioning the energy among the protosolitons, but the exponential localization of the daughter solitons means they rapidly cease to interact.

Generalizing from the particular cases displayed in Figs. 2 and 3, we find very similar behavior over a wide range of parameter values. For both models the sign of l, which defines the direction of the angular momentum, fixes the orientation of the soliton trajectories. The number of daughter solitons depends strongly on the azimuthal index l, but relatively weakly on all other parameters.

While we believe that our results are conceptually and pedagogically interesting, independent of direct experimental verification, it is naturally of interest to address the question of experimental observation of these or related phenomena. We already mentioned the work of Shih *et al.* [11], and several other recent papers report experiments which relate in some way to our scheme and are thus generally encouraging, though in each case there are important and interesting differences.

Tikhonenko *et al.* report experiments in rubidium vapor (a saturable self-focusing medium) [12,13]. They observed, and confirmed in simulations, fragmentation of beams with a phase dislocation. They did not consider the possibility of doughnut solitons. Their experimental results were quite strongly affected by the lack of azimuthal symmetry of their input beam, especially in the case $l = 2$ [13]. For the case of $l = 1$ their results [12] are quite similar to ours, with two daughter solitons produced. A side view indicates straight-line trajectories with no evidence of interaction forces leading to spiraling.

In the $\chi^{(2)}$ case, Torner and Petrov [14] recently described numerical simulation for the case where the input was a Laguerre-Gaussian for E_1 with $E_2 = 0$. They concentrated on the case $l = 1$. Typically three solitons were output, broadly in accord with our findings, though for quite different initial conditions. Stationary solutions such as doughnut solitons, we would argue, are the natural starting point for studies of more general input conditions. Finally, Fuerst *et al.* recently reported an experiment [6] quite close to our model, except that the input is "unrolled" to form an intense line focus. The observed filamentation into up to six stable solitons is encouraging for similar experiments with finite angular momentum.

In conclusion, we have shown the existence of a new kind of ringlike solitary wave, with finite orbital angular momentum. These are unstable on propagation, breaking into filaments which become solitons, whose number is strongly dependent on the input angular momentum. The solitons fly out tangentially from the initial ring, like free Newtonian particles, and their motion is accurately described using Newtonian conservation laws for energy, momentum, and angular momentum. This scenario is rather robust, with broadly similar phenomena occurring over a wide range of parameters, both in quadratically nonlinear and in self-focusing media.

This work was partially supported by EPSRC Grant No. GR/L 27916. D. V. S. acknowledges financial support from ORS award scheme.

*Electronic address: dmitry@phys.strath.ac.uk

[1] A. C. Newell, *Solitons in Mathematics and Physics* (SIAM, Philadelphia, 1985).
[2] A. Aceves *et al.*, J. Opt. Soc. Am. B **7**, 963 (1990); D. E. Edmundson and R. H. Enns, Phys. Rev. A **51**, 2491 (1995).
[3] J. J. Rasmussen and K. Rypdal, Phys. Scr. **33**, 481 (1986).
[4] A. V. Buryak, Y. S. Kivshar, and V. Steblina, Phys. Rev. A **52**, 1670 (1995).
[5] G. I. Stegeman, D. J. Hagan, and L. Torner, Opt. Quantum Electron. **28**, 1691 (1996).
[6] R. A. Fuerst *et al.*, Phys. Rev. Lett. **78**, 2756 (1997).
[7] L. Allen *et al.*, Phys. Rev. A **45**, 8185 (1992); N. R. Heckenberg *et al.*, Opt. Lett. **17**, 221 (1992); N. B. Simpson *et al.*, Opt. Lett. **22**, 52 (1997).
[8] K. Dholakia *et al.*, Phys. Rev. A **54**, R3742 (1996).
[9] M. G. Vakhitov and A. A. Kolokolov, Sov. Radiophys. **16**, 783 (1973); D. E. Pelinovsky, A. V. Buryak, and Y. S. Kivshar, Phys. Rev. Lett. **75**, 591 (1995).
[10] J. M. Soto-Crespo *et al.*, Phys. Rev. A **44**, 636 (1991); J. Atai, Y. Chen, and J. M. Soto-Crespo, Phys. Rev. A **49**, R3170 (1994).
[11] M. Shih, M. Segev, and G. Salamo, Phys. Rev. Lett. **78**, 2551 (1997).
[12] V. Tikhonenko, J. Christou, and B. Luther-Davies, J. Opt. Soc. Am. B **12**, 2046 (1995).
[13] V. Tikhonenko, J. Christou, and B. Luther-Davies, Phys. Rev. Lett. **76**, 2698 (1996).
[14] L. Torner and D. V. Petrov, Electron. Lett. **33**, 608 (1997).